THE JOURNAL OF PHYSICAL CHEMISTRY C
A JOURNAL OF THE AMERICAN CHEMICAL SOCIETY

pubs.acs.org/JPCC
Article

Nanoparticle Shape Effects on the SERS Properties of Small Conductive Bridges

Published as part of The Journal of Physical Chemistry C special issue "Celebrating 50 Years of Surface Enhanced Spectroscopy".

Giordano Toscano Paganoto, Marcia Laudelina Arruda Temperini, and Diego Pereira dos Santos*

Cite This: J. Phys. Chem. C 2024, 128, 15974−15984

Read Online

ACCESS | Metrics & More | Article Recommendations | Supporting Information

ABSTRACT: Surface-enhanced Raman scattering (SERS) allows for the vibrational spectroscopy study of a very small number of molecules, especially those located in the gap region separating two metal surfaces, where near-field enhancements are considerably large—the so-called SERS hot spots. The small number of molecules in the very localized hot spots permits the study of fundamental properties associated with SERS, such as the effect of plasmonic coupling on near-field enhancements. The engineering of hot spots can be achieved through molecular junctions. The careful analysis of the effects of hot spot shape and molecular conductances is of paramount importance for the correct interpretation of experimental results and the design of composite systems (nanoparticles and molecular junctions) for different experimental applications. In this work, we investigate these parameters for Au nanospheres and Au nanorods connected to a Au film by oligophenylenedithiol (OPD) molecules of different sizes. Our study permits the interpretation of hot spot shape (created by different nanoparticles) and molecular bridge conductance effects on SERS intensities as a function of gap size.

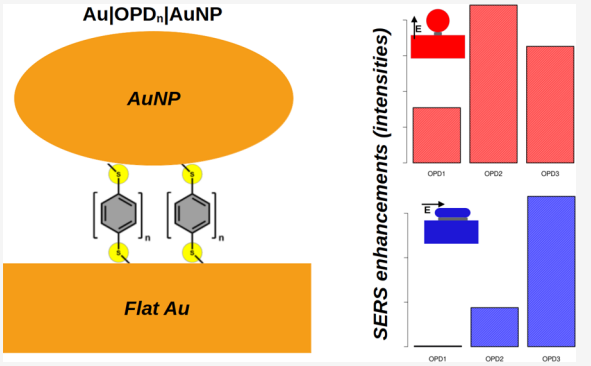

INTRODUCTION

Surface Enhanced Raman Scattering (SERS) is a widely used spectroscopic technique that is approaching its 50th year since the original observation.[1] In SERS, the inelastically scattered radiation by a probed molecule has its intensity enhanced by several orders of magnitude in comparison to normal Raman scattering. This effect is a result of the close proximity of molecules to nanostructured plasmonic metal surfaces such as gold and silver.[2−5] The near-field enhancements are especially pronounced in the gap between metal surfaces with coupled plasmonic modes, and such regions are usually referred to as hot spots.[3,6−8] The presence of such spots in a given SERS substrate allows for the analytical detection of ultralow analyte concentrations, even at single-molecule detection limits.[9−16] Besides such analytical power, it has been demonstrated that SERS signals can be used as a tool to investigate the plasmonic properties of metal nanoparticles, such as the field enhancement resonances[6,15] and their associated local statistical distributions,[17−19] the temperature effects due to plasmon relaxation,[20−22] plasmon modes interferences,[23−27] and charge-transfer plasmon modes.[28−30]

A key feature in SERS is the hot spot engineering. In the case of nanoparticles, the simplest approach is the use of molecular junctions bridging the gap between metal surfaces. The use of molecular groups that strongly interact with metal surfaces can be an efficient way of producing controlled hot spots. For example, the use of oligophenyleneimines (OPI)[31] or oligophenylenedithiols (OPD),[32] like benzene-1,4-dithiol, can be explored, which have been widely studied as molecular junction due to the possibility of creating a bridge between two metallic contacts.

The use of OPI or OPD molecules is of great importance for investigating the SERS properties of hot spots due to the possibility of controlling the gap size by changing the number of phenylene groups.[31] Such an approach allows for experimental control of hot spot properties to extract relevant information related to the fundamental properties of SERS. One SERS substrate that can be produced by the combination of metal nanoparticles and OPI (or OPD) is the nanoparticle-on-mirror (NPoM) construct, which consists of a plasmonic nanoparticle placed onto a metallic flat surface.[30,33−35] In this

Received: May 30, 2024
Revised: September 6, 2024
Accepted: September 9, 2024
Published: September 16, 2024

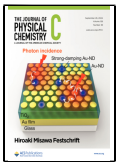

https://doi.org/10.1021/acs.jpcc.4c03587
J. Phys. Chem. C 2024, 128, 15974−15984

case, the junction can be created by molecular self-assembly prior to nanoparticle deposition.

Recently, we investigated the effect of controlling the gap size in the MPoM configuration by depositing gold nanorods (AuNR) on a gold flat surface.[31] The gap sizes in such systems were created using OPI of different sizes, ranging from approximately 2.2 nm up to 9.9 nm. Classical electrodynamics simulations based on DDA (discrete dipole approximation) for each MPoM showed that the excitation of the longitudinal plasmon mode within the AuNR leads to coupling with the underlying Au flat surface through an image-dipole interaction, which allows for concentration of field enhancements in the gap, thereby enabling strong SERS enhancements of OPI molecules. The simulated data were in good agreement with the experimental SERS intensity profile, indicating nearly constant SERS intensities for OPI molecules with 3−5 phenylene groups, followed by a steep decrease in intensities for longer gap sizes. However, the pure classical approach was not able to fully capture the observed intensity profile for the smaller OPI molecules, which showed an increase with the number of phenylene groups.

Cui et al.[30] and Benz et al.[29] demonstrated that the increase in molecular conductance leads to a blueshift of the observed plasmon resonance in NPoM systems composed of Au|OPD| gold nanospheres. The blueshift is argued to occur due to the formation of a charge transfer plasmon (CTP), where the molecular bridge allows for the charge associated with the plasmonic waves to be transferred between the nanoparticle and Au flat surface.

In this work, we explore the possible effect of charge transfer between metal surfaces on the SERS properties of NPoM systems with small conductive bridges. The investigated configurations were chosen to be of the type Au flat|OPDn| AuNP, where the AuNP (Au nanoparticle) geometries considered are Au nanospheres (AuNS) and Au nanorods (AuNRs). Three conductive bridges were considered with varying numbers of phenylene groups (n in OPDn): n = 1 (OPD1), n = 2 (OPD2), and n = 3 (OPD3).

METHODS

AuNR Synthesis. AuNR synthesis was performed following the protocol described by Scarabelli et al.[36] A seed solution was prepared at 29 °C by adding 25 μL of a 50 mM solution of $HAuCl_4{\cdot}3H_2O$ in 10 mL of a cetyltrimethylammonium bromide (CTAB) solution at a concentration of 100 mM. The mixture was left under stirring for 5 min. Then, 300 μL of a freshly prepared 10 mM $NaBH_4$ solution was added under vigorous stirring. The resulting seed solution showed a pale brown color.

The growth solution was obtained by adding 100 μL of a 50 mM $HAuCl_4{\cdot}3H_2O$ solution to 10 mL of a CTAB solution at a concentration of 100 mM. The mixture was left to rest for 10 min at 29 °C. Then, 75 μL of a 100 mM ascorbic acid solution was added, and the mixture was gently stirred until the color changed from yellow to colorless. 80 μL of a 10 mM $AgNO_3$ solution was added, and the mixture was gently stirred for a few seconds. The Ag_+ ions block the process of Au growth along the AuNR diameter, resulting in anisotropic nanoparticles.[37] Finally, the growth process of AuNR particles was performed by adding 120 μL of the seed solution to the growth solution, leaving the mixture to rest for 30 min at 29 °C.

AuNS Synthesis. AuNS particles were prepared as described by Perez-Pazos et al.[38] Briefly, a seed solution was prepared with a 20 mL aqueous solution containing $HAuCl_4{\cdot}3H_2O$ (0.25 mM) and sodium citrate (0.25 mM). 600 μL of $NaBH_4$ (100 mM) was added, keeping the solution under vigorous stirring for 1 h until the complete decomposition of $NaBH_4$. The growth solution was prepared by dissolving CTAB (to a final concentration of 100 mM) and KI (0.3 mg/g of CTAB), followed by the addition of 204 μL of a 103 mM $HAuCl_4{\cdot}3H_2O$ solution and 294 μL of a 100 mM ascorbic acid solution. Vigorous stirring was performed after each addition. The presence of iodide ions at low concentrations inhibits the growth of nanorods through adsorption on certain crystallographic faces of the Au nanoparticles from the seed solution. Finally, the growth process of AuNS was undertaken by adding 75 μL of the seed solution to the growth solution. After this last step, the mixture was left to rest for 48 h at 29 °C.

Preparation of Au|OPDn|AuNP Substrates. NPoM systems were prepared by self-assembly of OPDn and AuNP particles. First, the Au flat surfaces were prepared by deposition of a 100 nm thickness layer of Au on mica. The Au surfaces were cleaned using air plasma to remove organic surface contaminants that may prevent OPDn layer formation. After the cleaning process, the substrates were placed in a 1 mM ethanolic solution of OPDn for 24 h at room temperature. OPD1 (benzene-1,4-dithiol, 99%), OPD2 (biphenyl-4,4′-dithiol, 95%) and OPD3 (*p*-terphenyl-4,4″-dithiol, 95%) were purchased from Sigma-Aldrich. After that, the Au modified substrates were rinsed with ethanol and horizontally immersed in diluted (10×) colloidal suspensions of AuNP particles (AuNR or AuNS) in 1:4 acetonitrile/water mixture for 24 h to obtain the NPoM systems. It is well-known in the literature that a small amount of acetonitrile can partially remove the CTAB bilayer from the AuNP surface.[39,40]

Characterization. The characterizations of AuNR and AuNS nanoparticles were performed through transmission electron microscopy (TEM) using a JEOL JEM 2100 microscope at an accelerating voltage of 200 kV. To obtain TEM images, the nanoparticles were deposited drop by drop on a 300 mesh copper grid with Formvar/Carbon coating.

NPoM systems were characterized using a Thermo Fisher Quanta 650 FEG scanning electron microscope. The images were obtained with a secondary electron detector (SE) at an accelerating voltage of 5.0 kV.

SERS spectra were obtained using a Renishaw inVia Raman microscope equipped with a 100× objective lens with a numerical aperture (NA) of 0.85 and a diffraction grating with 600 lines/mm. The power of the exciting radiation was adjusted so that the power in the sample was approximately 2 mW. To acquire the spectra, a mapping was carried out with dimensions of 20 μm × 20 μm, obtaining a total of 441 spectra in each scan. The mappings were performed with the grating in static mode, which allows the collection of spectra in the range of approximately 900−1750 cm^{-1}. To study the effect of molecular conductance and gap size, the area under the band at ca. 1600 cm^{-1} was measured. All collected spectra were normalized by the intensity of the Si Raman scattering band at ca. 520 cm^{-1} for each incident laser wavelength used (633 and 785 nm). This normalization eliminates interferences from other factors, such as system alignment deviations or detector response curves.

Statistical Analysis. The SERS intensities were analyzed by boxplot, analysis of variance (ANOVA) and Tukey honestly significant difference (HSD).[41] All such statistics and data

https://doi.org/10.1021/acs.jpcc.4c03587
J. Phys. Chem. C 2024, 128, 15974−15984

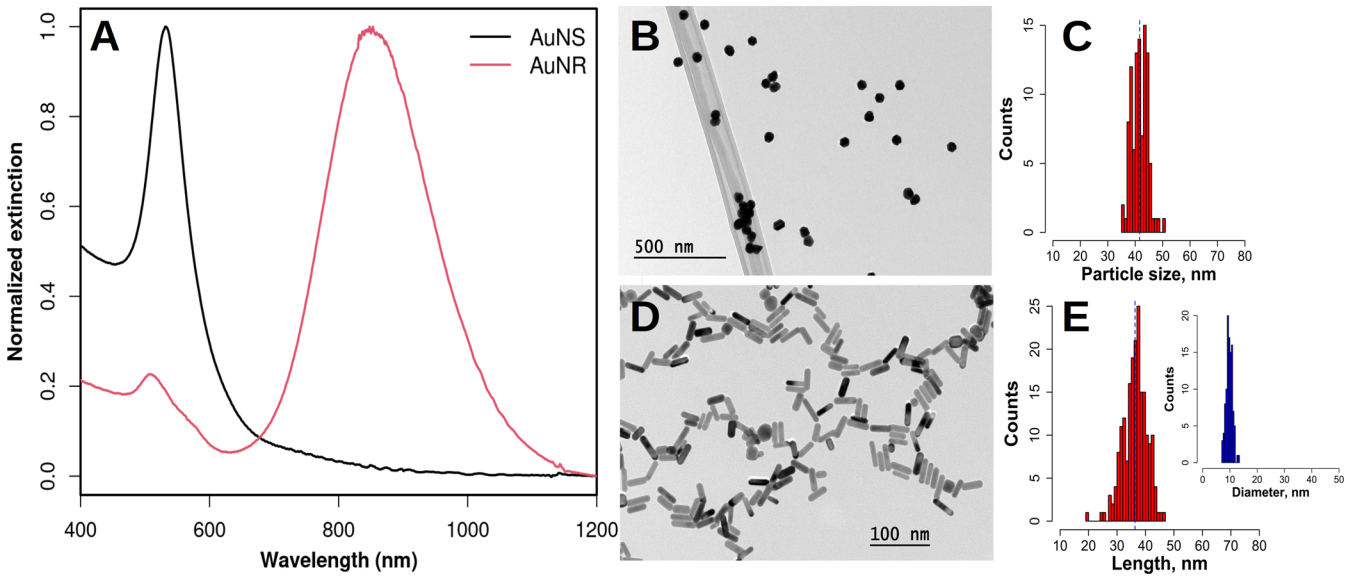

Figure 1. (A) Extinction spectra of AuNS (black) and AuNR (red) colloid samples. (B, C) show the TEM image of AuNS particles and the diameter distribution, respectively. (D) shows the TEM image of AuNR particles. (E) presents the size distribution for the AuNR length (red) and diameter (blue).

treatment were performed using the R software for statistical computing.[42]

Boundary Element Method (BEM). The plasmonic properties of NPoM systems were simulated using the MNPBEM17 toolbox developed by Hohenester and Trügler.[43] To simulate the effect of the Au substrate on the plasmonic properties of the nanoparticles, a cylinder was used following the criterion proposed by Malinsky et al.,[44] which was also used in our previous work.[31] Since the metallic surface is simulated by a cylinder with nanometric dimensions and presents an optical response, this contribution is constant and does not compromise the interpretation of the results. For Aul OPDn|AuNS NPoM systems, the molecular junctions were represented by a cylinder with a diameter of 2 nm and a height equal to the length of the OPD*n* molecule. In the case of AuNR, a block was used with lateral dimensions equal to the diameter and length of the rod and a height equal to the length of the OPD*n*. The dielectric function of OPD*n* was simulated considering the molecular conductance,[45,46] while the dielectric function of gold was taken from Johnson and Christy's experimental compilation.[47]

RESULTS AND DISCUSSION

Characterization of the prepared AuNS and AuNR particles is presented in Figure 1. The experimental extinction spectra indicate the well-known behavior expected for Au nanospheres, with a single dipolar plasmonic resonance (black line in Figure 1A), and for Au nanorods, with two plasmonic modes (red line in Figure 1A): longitudinal (ca. 800 nm), i.e., dipolar oscillation along the rod's main axis, and transversal (ca. 500 nm), i.e., along the axis that describes the rod's diameter. Interestingly, the modes near 500 nm for both samples present reasonably narrow bands, suggesting a narrow distribution of particle size and shape. Further evidence for the successful synthesis of AuNS and AuNR particles can be obtained from the TEM images (Figure 1B,1D), which clearly show the spherical and rod-like shapes. The images indicate that both syntheses lead to small variations in nanoparticle size and shape distributions. This is, indeed, corroborated by the

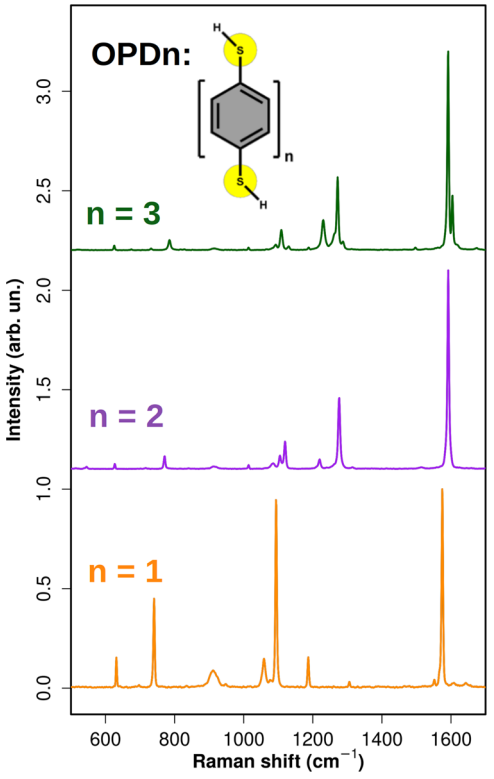

Figure 2. FT-Raman (1064 nm excitation) for the different OPD*n* in solid state: OPD1 (n = 1), OPD2 (n = 2) and OPD3 (n = 3).

Table 1. Conductance Values, G and OPD*n* Lengths[a]

OPD*n*	G/G_0	gap (nm)
OPD1	2.13	1.25
OPD2	0.48	1.69
OPD3	0.09	1.87

[a] $G_0 = \frac{2e^2}{h}$. The data was extracted from Xie et al.[45]

https://doi.org/10.1021/acs.jpcc.4c03587
J. Phys. Chem. C 2024, 128, 15974−15984

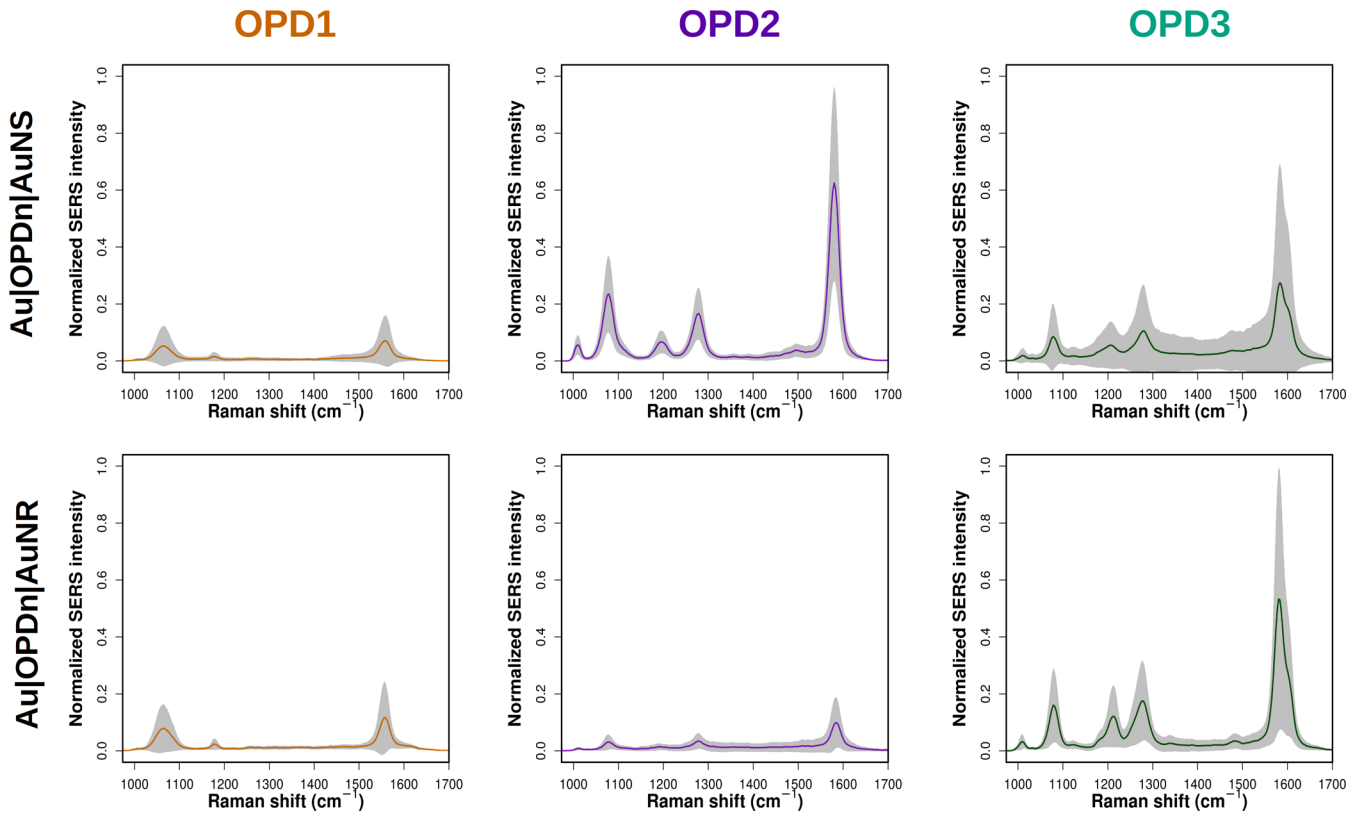

Figure 3. Average SERS spectra from the mapping at 633 nm excitation for different Au|OPD*n*|AuNP systems. Each column represents a different size OPD*n*: OPD1 (left, orange), OPD2 (middle, purple), and OPD3 (right, green). The gray shadow represents the standard deviation from the average spectrum. The two rows indicate different AuNPs: AuNS (first row) and AuNR (second row). The intensities are normalized by the most intense spectrum in the entire data set for a given particle shape.

distributions of particle sizes extracted from TEM image analysis, which are shown in Figure 1C,1E. For the AuNR sample, the two distributions are associated with the AuNR length (red histogram, average: 38.0 ± 4.3 nm) and diameter (blue histogram, average: 9.8 ± 1.1 nm). The AuNS sample presented an average size of 41.6 ± 3.1 nm.

The nanoparticles were used for the preparation of NPoM systems by deposition onto 100 nm-thick Au films. Prior to nanoparticle deposition, the Au substrate surface was modified by self-assembly of OPDn molecules of different sizes characterized by the number of phenylene groups. In this work, we explored OPDn with up to 3 groups (OPD1, OPD2, and OPD3). The inserts in Figure 2 present the molecular structures of OPD1, OPD2, and OPD3 used in this work.

OPDn molecules are well-known for their properties as conducting bridges in the gap between two metal surfaces (Au, for instance).[32] We have explored similar systems of oligophenyleneimines (OPI) as conducting bridges between a gold surface and AuNR particles.[31] In that study, we observed an increase in OPI SERS intensities with OPI length for the smallest bridge sizes (up to 3 phenylene groups) and a decrease with bridge size for larger OPI (more than 5 phenylene groups). Although we were successfully able to explain the SERS behavior in the long gap size regime, the increase in SERS intensities for small gaps was not captured by our computational simulations. In this work, we investigate this small gap size regime and the effect of nanoparticle shape on the observed SERS behavior.

Figure 2 shows the experimental FT-Raman (using 1064 nm excitation laser) as a function of OPDn molecular wire size. The most intense band in the spectra (1574 cm^{-1} for OPD1 and 1592 cm^{-1} for OPD2 and OPD3) is assigned to a ν_{8_a} mode, while the ν_1 can be observed at ca. 1090 cm^{-1}.[48,49]

As it can be observed in Figure 2, the increase in OPD*n* size leads to an increase in the relative band intensities for ν_{8_a} and ν_1 modes. We believe this effect is related to the increase in the number of phenylene groups. Table 1 presents the conductance values for each OPD*n* molecule. Interestingly, the conductance data shows an opposite trend if compared to the relative Raman intensities for modes ν_{8_a} and ν_1.

The SERS spectra obtained at 633 nm excitation for the different Au|OPDn|AuNP systems, with AuNP being either AuNS or AuNR and OPDn being OPD1, OPD2, or OPD3, were collected in mapping mode. The average spectra (excluding noise-only spectra) are presented in Figure 3. The data are shown in terms of normalized intensity, where the most intense spectrum in the entire data set (OPD1, OPD2, and OPD3) for a given nanoparticle structure (AuNS or AuNR) was used for normalization.

The gray areas around the average spectra in Figure 3 show the standard deviations. The results suggest that strong intensity fluctuations are observed among the SERS spectra in the mapped area of the Au|OPDn|AuNP systems. This is a result of local structural changes in terms of AuNP aggregation state as well as the possible effect of Au substrate surface roughness. Even though the Au substrate was previously treated by an annealing procedure to reduce roughness, fractal-like nanostructures can still be observed on the Au film (see

https://doi.org/10.1021/acs.jpcc.4c03587
J. Phys. Chem. C 2024, 128, 15974−15984

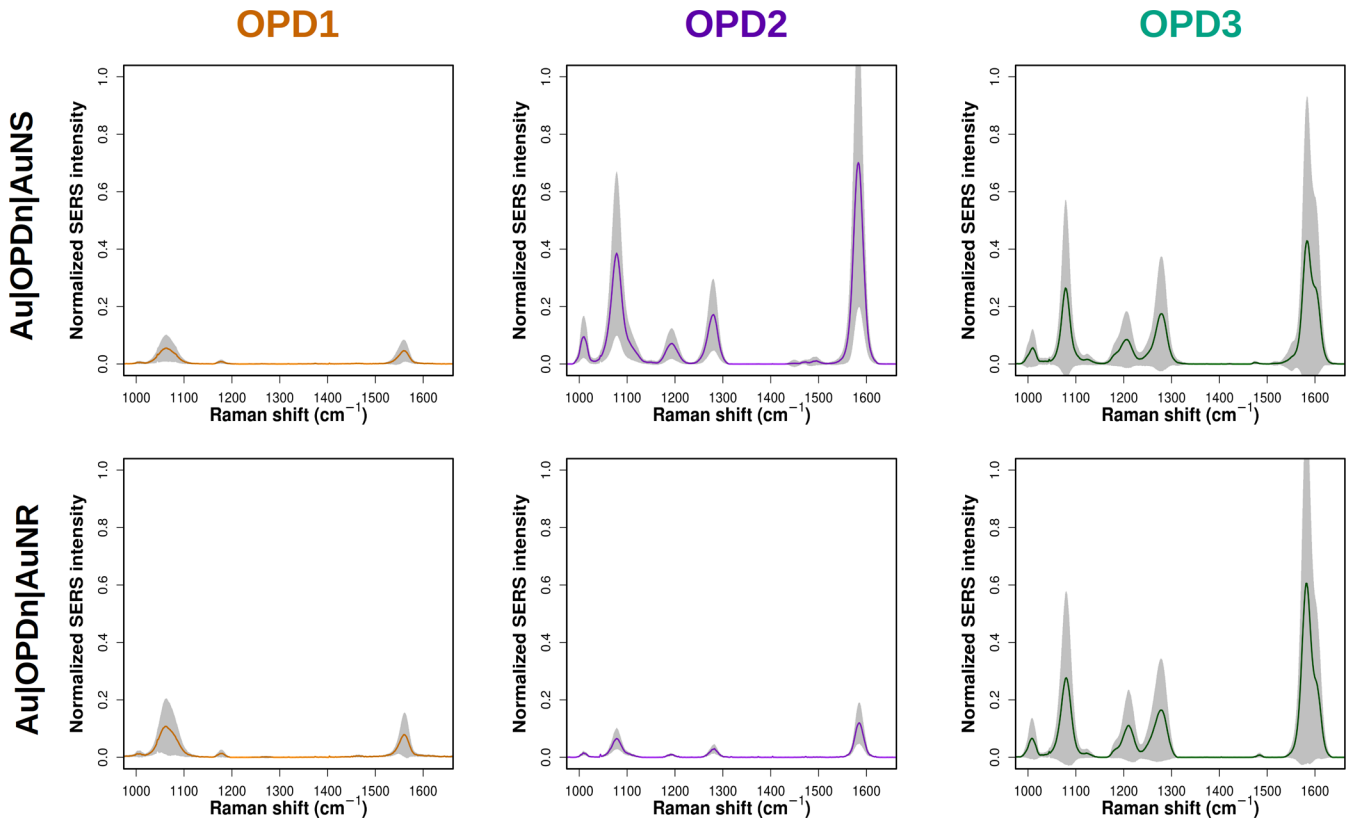

Figure 4. Average SERS spectra from the mapping at 785 nm excitation for different Au|OPDn|AuNP systems. Each column represents a different size OPDn: OPD1 (left, black), OPD2 (middle, red), and OPD3 (right, blue). The gray shadow represents the standard deviation from the average spectrum. The two rows indicate different AuNPs: AuNS (first row) and AuNR (second row). The intensities are normalized by the most intense spectrum in the entire data set for a given particle shape.

scanning electron microscopy images of the Au|OPDn|AuNP systems in the SI file).

The use of 785 nm excitation (Figure 4) leads to similar results as those in Figure 3, albeit with a lower total SERS intensity. Another difference between 633 and 785 nm excitation results is the overall change in relative intensities for modes ν_1 and ν_{8_a}. For instance, at 633 nm, the intensity for the ν_{8_a} mode in OPD1 is slightly larger than for ν_1. At 785 nm, however, the opposite result is observed. In fact, for all Au|OPDn|AuNP systems, the ν_{8_a}/ν_1 intensity ratio is, on average, smaller at 785 nm. This observation indicates plasmonic near-field resonance effects,[6,15] which could be a result of plasmonic resonances closer to 633 nm than to the 785 nm laser line. In fact, in our previous study, DDA simulations indicated such behavior for a single AuNR on top of Au surfaces.[31] If this interpretation is correct, we could assume that most of the SERS spectra are due to single particles in Au|OPDn|AuNP configurations when the excitation is at 633 nm, although we cannot exclude contributions from structures formed by aggregated AuNPs. The SEM image in the SI file shows a reasonable agreement with this interpretation. The lower total intensities for 785 nm are, therefore, a direct result of resonance conditions. At this longer wavelength, aggregates are of paramount importance for the appropriate description of absolute SERS intensities.

The large intensity fluctuations in the data presented in Figures 3 and 4 are highlighted by the standard deviation calculations for each Raman shift. In order to analyze any possible trend in the data it is important to compute how statistically significant are the differences among observed intensities. For this goal, we performed a boxplot analysis for the intensities of ν_{8_a} mode for Au|OPDn|AuNS and Au|OPDn|AuNR systems using both 633 and 785 nm excitation sources.

The lower and upper limits for the boxes in Figure 5 represent the second (Q2) and third (Q3) quartiles, which means that 25−75% of the intensity data is contained inside the box region. The line inside the box represents the median. If we take the data for Au|OPD2|AuNS at 633 nm excitation as an example, it is possible to observe that most of the data is distributed above the median. The horizontal lines below and above the boxes are the first (Q1) and fourth (Q4) quartiles, which correspond to Q2−1.5xIQR and Q3 + 1.5xIQR, respectively, where IQR is the interquartile range (Q3-Q2). The dots represent data classified as outliers in this analysis.[50] Therefore, we argue that this analysis better captures the intensity variations, as it presents not only the average intensities but also the shape of the intensity distribution. Taking the AuNS data at 633 nm excitation as an example, it is possible to observe an increase in intensity from OPD1 to OPD2, followed by a decrease in OPD3. On the other hand, the systems composed of AuNR nanoparticles, when excited at 633 nm, show a completely different intensity profile: OPD3 presented the highest intensities, while OPD1 and OPD2 showed similar but lower intensities. Changing excitation from 633 to 785 nm leads to intensity profiles that resemble the observations for 633 nm, although with considerably higher data dispersion. To ensure the statistical significance of these results, we also performed a Tukey honestly significant

https://doi.org/10.1021/acs.jpcc.4c03587
J. Phys. Chem. C 2024, 128, 15974−15984

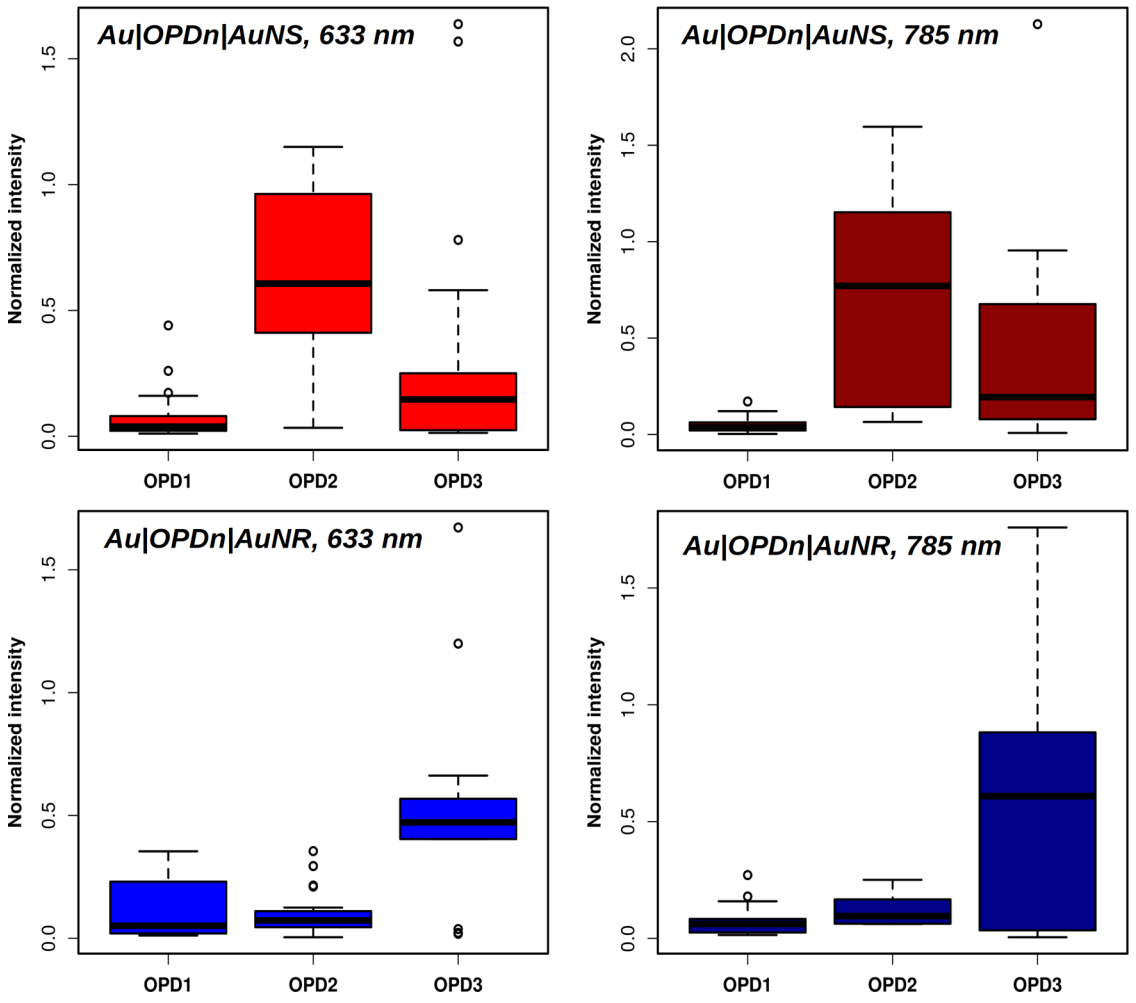

Figure 5. Boxplot analysis for the ν_{8_a} mode intensities for OPD1-OPD3. The first row presents the SERS intensities in the Au|OPDn|AuNS system for 633 nm (left) and 785 nm (right) excitation. The second row presents the same data for Au|OPDn|AuNR using 633 nm (left) and 785 nm (right) excitation.

difference (Tukey HSD) analysis, which measures the differences among the average values for SERS intensity in each sample/experiment. The results are presented in Figure 6.

The Tukey HSD analysis in Figure 6 indicates how different the average SERS intensities are for the three possible pairs (OPD2-OPD1, OPD3-OPD1, and OPD3-OPD2). The range around each difference is the confidence interval (related to the mean square error for all the data, taken from ANOVA results) and is a measure of significance in the differences. Taking the AuNR systems with 633 nm as an example, for the pair OPD1 and OPD2 the confidence interval passes through 0, which means that the difference between the average values is not statistically significant. On the other hand, there are significant differences between the data for the pairs OPD3-OPD1 and OPD3-OPD2. This is in agreement with the data in Figures 3 and 5. The Tukey analysis also reinforces the statistical differences between OPD1, OPD2, and OPD3 for the AuNS system at 633 nm excitation. The results for 785 nm show the same trend as for 633 nm excitation, but with larger dispersions. Therefore, we conclude that the change in the molecular wire leads to the same intensity profiles, regardless of the laser excitation, with the differences only related to the nanoparticle shape. More detailed results from the Tukey HSD analysis is presented in the supporting inormation (SI) file.

The Au|OPD*n*|AuNR system shows small relative intensities for OPD1 and OPD2 and a sudden intensity increase for OPD3. The result is in agreement with our previous result using OPI instead OPD as molecular junctions.[31] One could argue that such intensity behavior is, in fact, a direct result of the increase in Raman cross-section with the number of oligophenylene groups (which were indeed observed in normal Raman). Although, we cannot exclude such contribution from the data, there are evidence that suggest that other effects are in place:

- the SERS intensities do not always increase with the molecular junction size (as we observed for OPI junctions) in our previous investigation;
- the SERS results for AuNS particles show a completely different intensity profile with OPDn length.

The AuNS system shows an increase in intensity from OPD1 to OPD2 with a subsequent decrease from OPD2 to OPD3. The observation that changing the excitation wavelength does not lead to differences in the SERS intensity profiles with OPD*n* length is quite interesting. The gap size variation leads to changes in the dipole-image coupling strengths. The experimental results show that such effects are the same whether we probe single (or small aggregates) at 633 nm or larger aggregates at 785 nm, indicating that the results

https://doi.org/10.1021/acs.jpcc.4c03587
J. Phys. Chem. C 2024, 128, 15974−15984

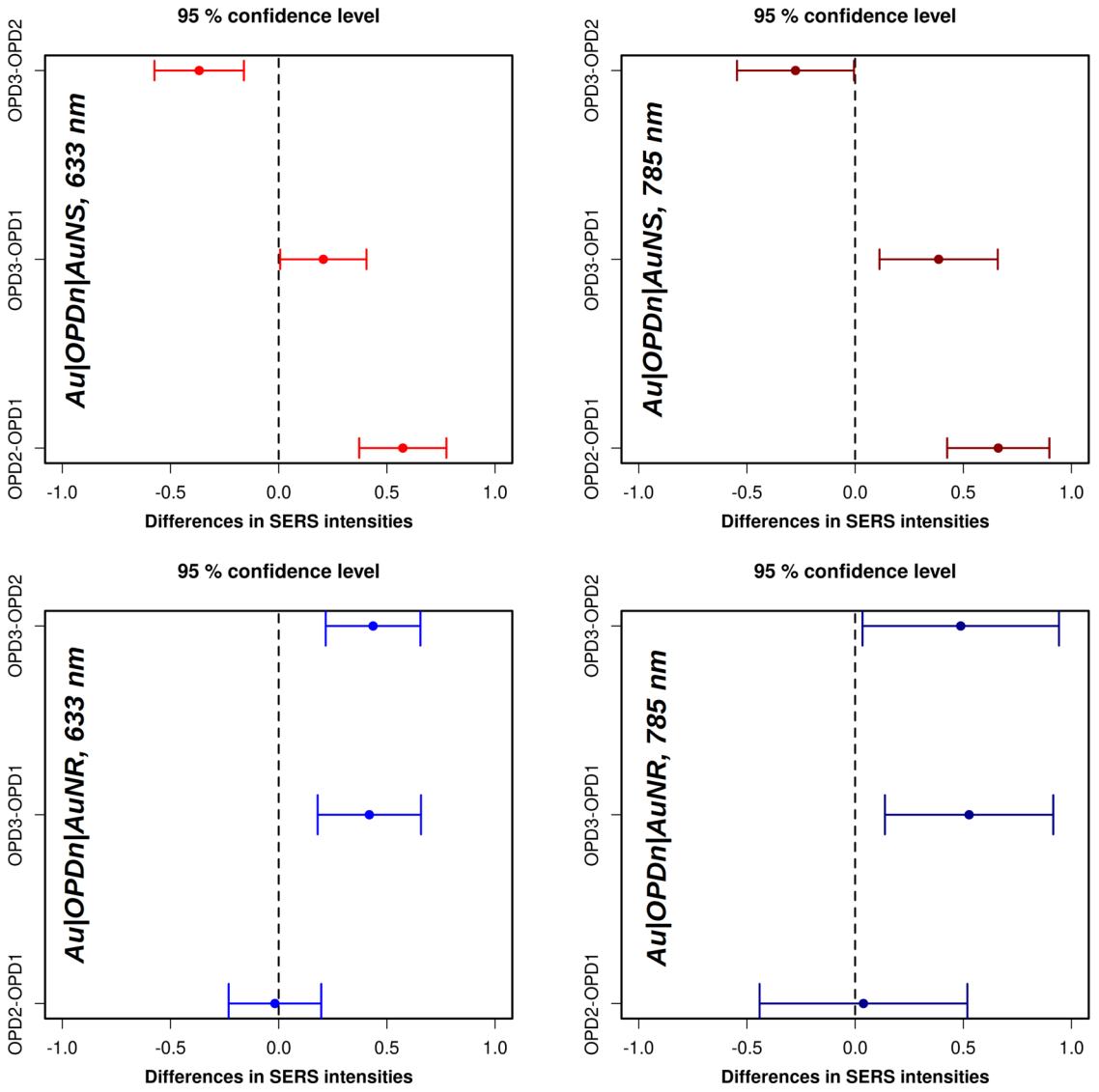

Figure 6. Tukey analysis for the differences between all average SERS intensities. The horizontal lines represent the confidence interval, while the vertical dashed lines indicate information that are statistically identical.

are mostly dependent on the hot spot properties due to nanoparticle shape. To aid in the interpretation of such shape-related effects, we performed BEM simulations to model the different Au|OPDn|AuNP systems. To include conductance effects associated with the molecular wires, we assumed a dielectric cylinder of radius r representing the molecular connections between the Au surface and the AuNS particle. The radius of this dielectric cylinder was assumed to be 2 nm.[30] A similar approach was taken for the AuNR systems, with the change from a cylinder to a parallelepiped with AuNR length excluding the hemispherical caps. A schematic representation can be found in the inset of Figure 8 by the gray shadows between the AuNP and the nanoparticle.

The local frequency-dependent dielectric function of this conducting region was simulated according to the following equation[30]

$$\epsilon(\omega) = n_0^2\left[1 + \frac{4\pi\kappa}{\omega}\right] \tag{1}$$

where κ is the conductivity in the junction, a parameter related to the conductance

$$G = \kappa\frac{\pi r^2}{d} \tag{2}$$

The parameters r and d are the radius and height of the conducting cylinder. d was taken as the OPDn sizes (Figure 2). The conductance values used in this approach are listed in Table 1. Each surface element in BEM has two possibilities for the external dielectric function: air (as the surrounding medium) or the conducting material. During the simulation, we ensure correctly identifying the surrounding dielectrics for each surface element in the meshed surfaces (see SI file).

The SERS intensities in each junction were simulated in terms of the SERS enhancement factor (F) according to the E^4 approximation

$$F \approx \left(\frac{|E|_{\text{local}}}{|E|_0}\right)^4 \tag{3}$$

where the values of F were calculated along the dashed lines at $y = 0$ in Figure 7. The example presented in Figure 7 is for Au|OPD1|AuNS and Au|OPD1|AuNR illuminated with 633 nm.

https://doi.org/10.1021/acs.jpcc.4c03587
J. Phys. Chem. C 2024, 128, 15974−15984

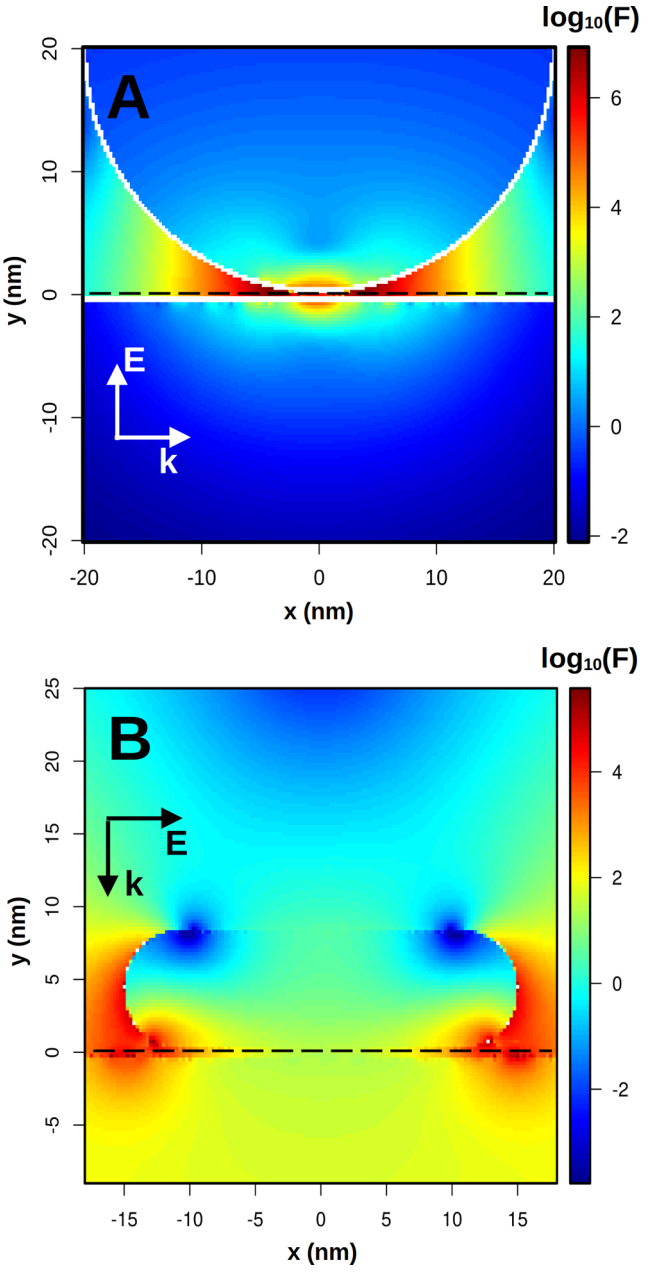

Figure 7. Enhancement factor (F) maps calculated for a plane passing through AuNP and hot spot centers. The F values were calculated according to the eq 3.

The incident wave polarization was taken as perpendicular and parallel to the Au surface for AuNS and AuNR particles, respectively (see insert of Figure 8).

The field enhancement in the conducting region for AuNR (Figure 7B) presents a drastic drop when compared to the regions below the hemispherical caps. The same effect can also be observed in the AuNS junction, although in a more limited region due to the nanoparticle geometry. This decrease in local field can be a result of charge transfer effects due to the molecular junction, which can be corroborated by the analysis of charge distribution (Figures S3 and S4 in SI file), which show considerable decrease in the conducting region. To account for the SERS enhancement for OPDn in such conducting regions, we calculated the average enhancement factor along the dashed lines in Figure 7, which is presented in Figure 8, for different excitation geometries.

The dashed lines around Figure 8B,8C are used to indicate the excitation scheme that yielded the largest enhancement factors. The comparison between the average enhancement factor at the HS and the SERS intensities indicates a good correlation, especially for Au|OPD*n*|AuNS systems. We were able to model the same profile observed in the experimental data in terms of gap size effect on SERS intensity. It is worth mentioning that this profile is slightly changed for 785 nm in the simulated results, with a lower relative intensity between OPD2 and OPD1 (see Figure S5 in SI file). A possible reason for that is the contribution of aggregates in the experimental data, which is not considered in our simple single-particle model. The Au|OPDn|AuNR enhancement factor shows a result that resembles the experimental data, in which the OPD1 and OPD2 signals are considerably lower than OPD3. The simulations for 785 nm are also very close to the experimental data. It is worth mentioning that the observed result is also in qualitative agreement with our experimental observation for OPI molecular junction.[31] Therefore, the simulated model correctly captures the essence of the experimental data, with the benefit of providing us a physical interpretation of the results in terms of charge transfer effects.

The AuNR geometry allows a greater degree of communication between both Au surfaces and, therefore, is more prone to such field depletion than the AuNS particle, for which the higher surface curvature around the hot spot leads to electron communication to a lesser extent. In fact, the AuNS profile is a direct superposition of two opposing effects: the near-field concentration (which increases for smaller OPD*n* sizes) and the field depletion due to charge transfer (which also increases for smaller OPD*n* sizes). We argue that both effects occur in each particle shape. However, due to the smaller electrical contact, the near-field damping effect for AuNS due to charge transfer is decreased and can only be observed in very high conducting bridges such as the OPD1 system. For higher electrical contacts, the near-field depletion can more easily be observed even for OPD2. As the conduction in the junction decreases, the effects of near-field concentration dominate. This effect is already the dominant one in the comparison between Au|OPD2|AuNS and Au|OPD3|AuNS, possibly due to the higher surface curvatures in the hot spot. As we were able to observe in our previous work, the MPoM systems using AuNR also permit the observation of lower field concentration in the hot spot with increasing gap size (OPI in that case).[31]

CONCLUSIONS

In this study, we investigated the SERS response of MPoM systems of the type Au|OPD*n*|AuNP, where the contact between a flat Au surface and AuNPs is produced by molecular junctions of different sizes (OPD1, OPD2, and OPD3), where the sizes are related to the number of phenylene groups. This study is a follow-up of a previous investigation where the experimental results for AuNR were explained in terms of near-field concentrations and their relationship with gap size. However, we were not able to explain the experimental observation of increasing SERS intensity with gap size for small molecular bridges. By including the possibility of charge transfer through the molecular bridge, we were able to fully reproduce the experimental results at these small bridge limits for AuNS and AuNR particles.

https://doi.org/10.1021/acs.jpcc.4c03587
J. Phys. Chem. C 2024, 128, 15974−15984

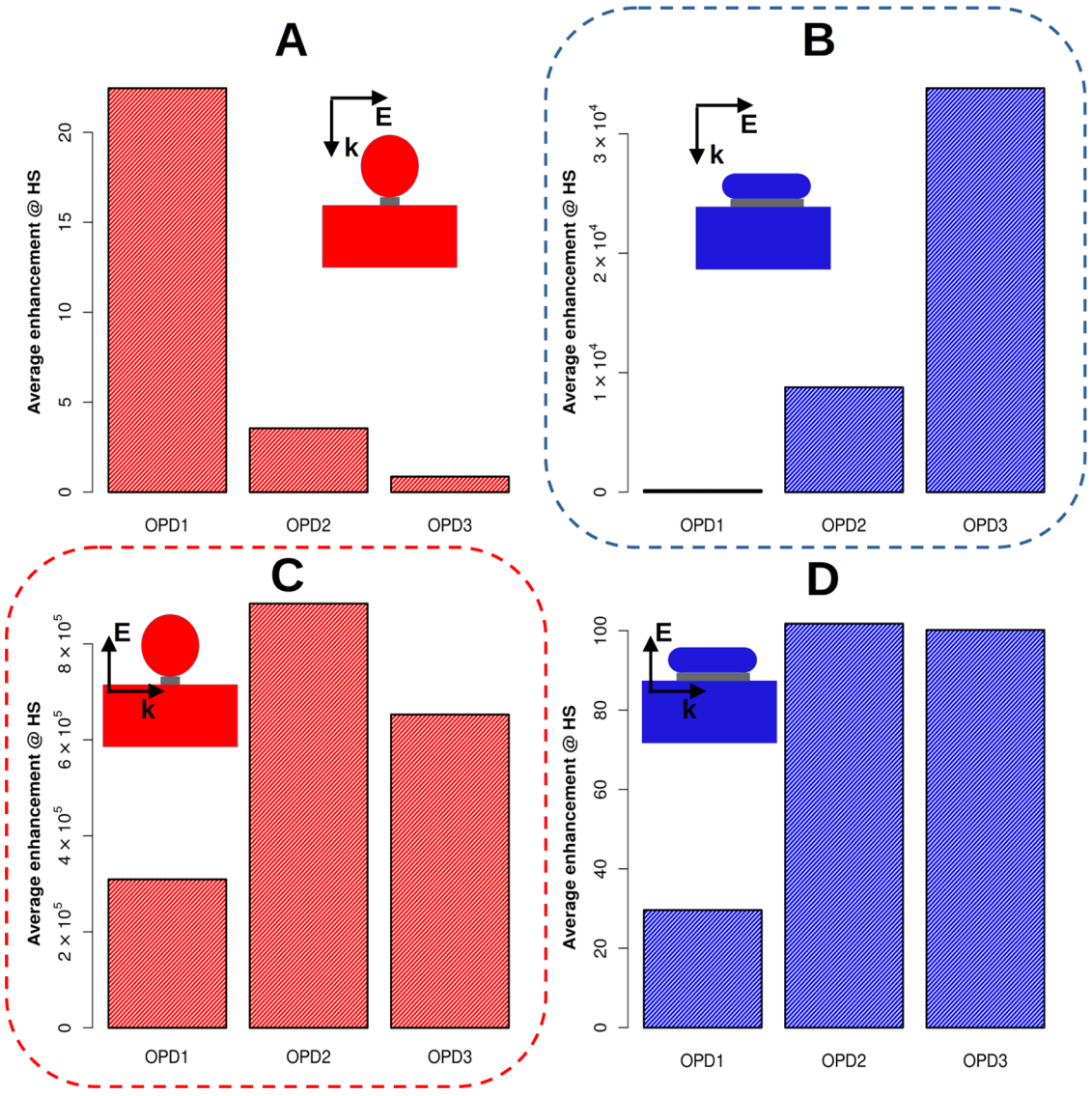

Figure 8. BEM-simulated average SERS enhancement factors (E^4 approximation) at the HS region (gray shadow) for Au|OPDn|AuNS (A, C) and Au|OPDn|AuNR (B, D). The simulations were performed at 633 nm excitation. The light polarizations (vectors **E**) and propagation directions (vectors **k**) are indicated on the figure schemes. The dashed boxes highlight the excitation configurations that yield the highest SERS enhancements.

The observed results and interpretations highlight the importance of considering the choice of nanoparticle shape for molecular junction investigations by the SERS effect. It is important to take into account not only the dipole-image coupling in MPoM systems but also the electrical contact conditions. Therefore, our results suggest that a SERS study aiming to explore molecular conduction should be performed with MPoM systems with large electrical contacts, conditions that are more sensitive to changes in conductance. On the other hand, an investigation in which the molecular junction is used only to produce controlled hot spots (for gap size effects investigation, for instance) should be performed with minimal effects from charge transfer, a condition that is better suited for low electrical contact metal nanoparticle shapes.

■ ASSOCIATED CONTENT

Supporting Information

The Supporting Information is available free of charge at https://pubs.acs.org/doi/10.1021/acs.jpcc.4c03587.

Microscopy images, further sample treatment information and SERS/BEM simulation results for 785 nm excitation (PDF)

■ AUTHOR INFORMATION

Corresponding Author

Diego Pereira dos Santos − *Institute of Chemistry, State University of Campinas, 13083-862 Campinas, Brazil;* orcid.org/0000-0001-9468-7293; Email: santosdp@unicamp.br

Authors

Giordano Toscano Paganoto − *Institute of Chemistry, University of São Paulo, 05508-000 São Paulo, Brazil*

Marcia Laudelina Arruda Temperini − *Institute of Chemistry, University of São Paulo, 05508-000 São Paulo, Brazil;* orcid.org/0000-0003-4655-6891

Complete contact information is available at: https://pubs.acs.org/10.1021/acs.jpcc.4c03587

Funding

The Article Processing Charge for the publication of this research was funded by the Coordination for the Improvement of Higher Education Personnel—CAPES (ROR identifier: 00x0ma614).

Funding

The Article Processing Charge for the publication of this research was funded by the Coordination for the Improvement of Higher Education Personnel - CAPES (ROR identifier: 00x0ma614).

Notes

The authors declare no competing financial interest.

■ ACKNOWLEDGMENTS

The authors would like to thank CNPq (405087/2021-7), FAPESP (2016/21070-5, 2022/11983-4) and FAEPEX/UNICAMP (3034/23) for supporting this work.

■ REFERENCES

(1) Fleischmann, M.; Hendra, P.; McQuillan, A. Raman spectra of pyridine adsorbed at a silver electrode. *Chem. Phys. Lett.* **1974**, *26*, 163−166.
(2) Aroca, R.; Rodriguez-Llorente, S. Surface-enhanced vibrational spectroscopy. *J. Mol. Struct.* **1997**, *408*−*409*, 17−22.
(3) Ru, E. C. L.; Etchegoin, P. G. *Principles of Surface-Enhanced Raman Spectroscopy And Related Plasmonic Effects*; Elsevier: Amsterdam, 2008.
(4) dos Santos, D. P.; Temperini, M. L. A.; Brolo, A. G. *Introduction to Plasmonics*; Pan Stanford, 2015; pp 275−317.
(5) Alves, R. S.; Mazali, I. O.; dos Santos, D. P. *Plasmonics-Based Optical Sensors and Detectors*; Jenny Stanford Publishing: New York, 2023; pp 277−316.
(6) dos Santos, D. P.; Temperini, M. L. A.; Brolo, A. G. Mapping the Energy Distribution of SERRS Hot Spots from Anti-Stokes to Stokes Intensity Ratios. *J. Am. Chem. Soc.* **2012**, *134*, 13492−13500.
(7) Litz, J. P.; Camden, J. P.; Masiello, D. Spatial, Spectral, and Coherence Mapping of Single-Molecule SERS Active Hot Spots via the Discrete-Dipole Approximation. *J. Phys. Chem. Lett.* **2011**, *2*, 1695−1700.
(8) Shahbazyan, T. V.; Stockman, M. I. *Plasmonics: Theory and Applications*; Springer: Netherlands: Dordrecht, 2013.
(9) Nie, S. M.; Emory, S. R. Probing Single Molecule and Single Nanoparticles by Surface-Enhanced Raman Scattering. *Science* **1997**, *275*, 1102−1106.
(10) Kneipp, K.; Wang, Y.; Kneipp, H.; Perelman, L. T.; Itzkan, I.; et al. Single Molecule Detection Using Surface-Enhanced Raman Scattering (SERS). *Phys. Rev. Lett.* **1997**, *78*, No. 1667.
(11) Le Ru, E. C.; Meyer, M.; Etchegoin, P. G. Proof of Single-Molecule Sensitivity in Surface Enhanced Raman Scattering (SERS) by Means of a Two-Analyte Technique. *J. Phys. Chem. B* **2006**, *110*, 1944−1948.
(12) Schmidt, M. M.; Farley, E. A.; Engevik, M. A.; Adelsman, T. N.; Bido, A. T.; Lemke, N. D.; Brolo, A. G.; Lindquist, N. C. High-Speed Spectral Characterization of Single-Molecule SERS Fluctuations. *ACS Nano* **2023**, *17*, 6675−6686.
(13) Zrimsek, A. B.; Chiang, N.; Mattei, M.; Zaleski, S.; McAnally, M. O.; Chapman, C. T.; Henry, A.-I.; Schatz, G. C.; Van Duyne, R. P. Single-Molecule Chemistry with Surface- and Tip-Enhanced Raman Spectroscopy. *Chem. Rev.* **2017**, *117*, 7583−7613.
(14) dos Santos, D. P.; Temperini, M. L. A.; Brolo, A. G. Intensity Fluctuations in Single-Molecule Surface-Enhanced Raman Scattering. *Acc. Chem. Res.* **2019**, *52*, 456−464.
(15) dos Santos, D. P.; Temperini, M. L. A.; Brolo, A. G. Single-Molecule Surface-Enhanced (Resonance) Raman Scattering (SE(R)-RS) as a Probe for Metal Colloid Aggregation State. *J. Phys. Chem. C* **2016**, *120*, 20877−20885.
(16) Kneipp, J.; Kneipp, H.; Kneipp, K. SERS—a single-molecule and nanoscale tool for bioanalytics. *Chem. Soc. Rev.* **2008**, *37*, 1052−1060.
(17) Le Ru, E. C.; Etchegoin, P. G.; Meyer, M. Enhancement factor distribution around a single surface-enhanced Raman scattering hot spot and its relation to single molecule detection. *J. Chem. Phys.* **2006**, *125*, No. 204701.
(18) Kiefl, E. J.; Kiefl, R. F.; dos Santos, D. P.; Brolo, A. G. Evaluation of Surface-Enhanced Raman Spectroscopy Substrates from Single-Molecule Statistics. *J. Phys. Chem. C* **2017**, *121*, 25487−25493.
(19) dos Santos, D. P. Statistical Analysis of Surface-Enhanced Raman Scattering Enhancement Distributions. *J. Phys. Chem. C* **2020**, *124*, 6811−6821.
(20) Baffou, G.; Quidant, R. Thermo-plasmonics: using metallic nanostructures as nano-sources of heat. *Laser Photonics Rev.* **2013**, *7*, 171−187.
(21) Baldwin, C. L.; Bigelow, N. W.; Masiello, D. J. Thermal Signatures of Plasmonic Fano Interferences: Toward the Achievement of Nanolocalized Temperature Manipulation. *J. Phys. Chem. Lett.* **2014**, *5*, 1347−1354.
(22) Baffou, G.; Cichos, F.; Quidant, R. Applications and challenges of thermoplasmonics. *Nat. Mater.* **2020**, *19*, 946−958.
(23) Yorulmaz, M.; Hoggard, A.; Zhao, H.; Wen, F.; Chang, W. S.; Halas, N. J.; Nordlander, P.; Link, S. Absorption Spectroscopy of an Individual Fano Cluster. *Nano Lett.* **2016**, *16*, 6497−6503.
(24) Santinom, A.; da Silva, M. A.; Villa, J. E. L.; Poppi, R. J.; Mazali, I. O.; dos Santos, D. P. Surface-enhanced Raman scattering (SERS) as probe of plasmonic near-field resonances. *Vib. Spectrosc.* **2018**, *99*, 34−43.
(25) Simoncelli, S.; Li, Y.; Cortés, E.; Maier, S. A. Imaging Plasmon Hybridization of Fano Resonances via Hot-Electron-Mediated Absorption Mapping. *Nano Lett.* **2018**, *18*, 3400−3406.
(26) Souza, K.; Teixeira-Neto, E.; Temperini, M.; dos Santos, D. Interplay Between Near-Field Properties and Au Nanorod Cluster Structure: Extending Hot Spots for Surface-Enhanced Raman Scattering. *J. Braz. Chem. Soc.* **2019**, *30*, 2624−2633.
(27) Alves, R. S.; Mazali, I. O.; dos Santos, D. P. Enhanced Surface Fields Driven by Fano Resonances in Silver Nanocube Dimers for Efficient Hot Electron Generation. *J. Phys. Chem. C* **2024**, *128*, 9182−9192.
(28) Tan, S. F.; Wu, L.; Yang, J. K.; Bai, P.; Bosman, M.; Nijhuis, C. A. Quantum plasmon resonances controlled by molecular tunnel junctions. *Science* **2014**, *343*, 1496−1499.
(29) Benz, F.; Tserkezis, C.; Herrmann, L. O.; De Nijs, B.; Sanders, A.; Sigle, D. O.; Pukenas, L.; Evans, S. D.; Aizpurua, J.; Baumberg, J. J. Nanooptics of molecular-shunted plasmonic nanojunctions. *Nano Lett.* **2015**, *15*, 669−674.
(30) Cui, X.; Qin, F.; Lai, Y.; Wang, H.; Shao, L.; Chen, H.; Wang, J.; Lin, H. Q. Molecular Tunnel Junction-Controlled High-Order Charge Transfer Plasmon and Fano Resonances. *ACS Nano* **2018**, *12*, 12541−12550.
(31) Souza, K. S.; dos Santos, D. P.; Andrade, G. F. S.; Pereira, M. B.; Teixeira-Neto, E.; Temperini, M. L. A. Molecular Wires Bridging Gaps between Gold Surfaces and Their Influence on SERS Intensities. *J. Phys. Chem. C* **2017**, *121*, 20937−20946.
(32) Iwane, M.; Fujii, S.; Kiguchi, M. Surface-Enhanced Raman Scattering in Molecular Junctions. *Sensors* **2017**, *17*, No. 1901.
(33) Langer, J.; de Aberasturi, D. J.; Aizpurua, J.; et al. Present and Future of Surface-Enhanced Raman Scattering. *ACS Nano* **2020**, *14*, 28−117.
(34) Dezfouli, M. K.; Hughes, S. Quantum Optics Model of Surface-Enhanced Raman Spectroscopy for Arbitrarily Shaped Plasmonic Resonators. *ACS Photonics* **2017**, *4*, 1245−1256.
(35) Chen, X.; Yang, Y.; Chen, Y.-H.; Qiu, M.; Blaikie, R. J.; Ding, B. Probing Plasmonic Gap Resonances between Gold Nanorods and a Metallic Surface. *J. Phys. Chem. C* **2015**, *119*, 18627−18634.
(36) Scarabelli, L.; Sánchez-Iglesias, A.; Pérez-Juste, J.; Liz-Marzán, L. M. A. Tips and Tricks" Practical Guide to the Synthesis of Gold Nanorods. *J. Phys. Chem. Lett.* **2015**, *6*, 4270−4279.

(37) Orendorff, C. J.; Murphy, C. J. Quantitation of Metal Content in the Silver-Assisted Growth of Gold Nanorods. *J. Phys. Chem. B* **2006**, *110*, 3990−3994.
(38) Pazos-Perez, N.; de Abajo, F. J. G.; Fery, A.; Alvarez-Puebla, R. A. From Nano to Micro: Synthesis and Optical Properties of Homogeneous Spheroidal Gold Particles and Their Superlattices. *Langmuir* **2012**, *28*, 8909−8914.
(39) Park, K.; Drummy, L. F.; Wadams, R. C.; Koerner, H.; Nepal, D.; Fabris, L.; Vaia, R. A. Growth Mechanism of Gold Nanorods. *Chem. Mater.* **2013**, *25*, 555−563.
(40) Bullen, C.; Zijlstra, P.; Bakker, E.; Gu, M.; Raston, C. Chemical Kinetics of Gold Nanorod Growth in Aqueous CTAB Solutions. *Cryst. Growth Des.* **2011**, *11*, 3375−3380.
(41) Barrows, R. D. Quantitative Comparison of Three Standardization Methods Using a One-Way ANOVA for Multiple Mean Comparisons. *J. Chem. Educ.* **2007**, *84*, 839−841.
(42) R Core Team. R: A Language and Environment for Statistical Computing, 2024 https://www.r-project.org/. (accessed September 6, 2024).
(43) Hohenester, U.; Trügler, A. MNPBEM — A Matlab toolbox for the simulation of plasmonic nanoparticles. *Comput. Phys. Commun.* **2012**, *183*, 370−381.
(44) Duval Malinsky, M.; Kelly, K. L.; Schatz, G. C.; Van Duyne, R. P. Nanosphere Lithography: Effect of Substrate on the Localized Surface Plasmon Resonance Spectrum of Silver Nanoparticles. *J. Phys. Chem. B* **2001**, *105*, 2343−2350.
(45) Xie, Z.; Bâldea, I.; Smith, C. E.; Wu, Y.; Frisbie, C. D. Experimental and Theoretical Analysis of Nanotransport in Oligophenylene Dithiol Junctions as a Function of Molecular Length and Contact Work Function. *ACS Nano* **2015**, *9*, 8022−8036.
(46) Pérez-González, O.; Aizpurua, J.; Zabala, N. Optical transport and sensing in plexcitonic nanocavities. *Opt. Express* **2013**, *21*, 15847−15858.
(47) Johnson, P. B.; Christy, R. W. Optical Constants of the Noble Metals. *Phys. Rev. B* **1972**, *6*, No. 4370.
(48) Ganbold, E.-O.; Joo, S.-W. Raman Spectroscopy of Biphenyl-4,4'-dithiol and p-Terphenyl-4,4"-dithiol on Gold Surfaces. *Bull. Korean Chem. Soc.* **2015**, *36*, 887−890.
(49) Suzuki, S.; Kaneko, S.; Fujii, S.; Marqués-González, S.; Nishino, T.; Kiguchi, M. Effect of the Molecule−Metal Interface on the Surface-Enhanced Raman Scattering of 1,4-Benzenedithiol. *J. Phys. Chem. C* **2016**, *120*, 1038−1042.
(50) Ferreira, J. E. V.; Pinheiro, M. T. S.; dos Santos, W. R. S.; da Silva Maia, R. Graphical representation of chemical periodicity of main elements through boxplot. *Educ. Quim.* **2016**, *27*, 209−216.

https://doi.org/10.1021/acs.jpcc.4c03587
J. Phys. Chem. C 2024, 128, 15974−15984